PLOS ONE

RESEARCH ARTICLE

Variability in phytoplankton biomass and effects of sea surface temperature based on satellite data from the Yellow Sea, China

Chunli Liu[1]*, Qiwei Sun[2,3], Qianguo Xing[4], Sufen Wang[5], Danling Tang[5], Donghe Zhu[6], Xiang Xing[1]*

1 Marine College, Shandong University (Weihai), Weihai, China, **2** State Key Laboratory of Tropical Oceanography, South China Sea Institute of Oceanology, Chinese Academy of Sciences, Guangzhou, China, **3** College of Earth and Planetary Sciences, University of Chinese Academy of Sciences, Beijing, China, **4** Yantai Institute of Coastal Zone Research, Chinese Academy of Sciences, Yantai, China, **5** State Key Laboratory of Tropical Oceanography, Guangdong Key Laboratory of Remote Sensing, South China Sea Institute of Oceanology, Chinese Academy of Sciences, Guangzhou, China, **6** Ocean College, Zhejiang University, Zhoushan, China

* chunliliu@sdu.edu.cn (CL); xingxiang@sdu.edu.cn (XX)

Citation: Liu C, Sun Q, Xing Q, Wang S, Tang D, Zhu D, et al. (2019) Variability in phytoplankton biomass and effects of sea surface temperature based on satellite data from the Yellow Sea, China. PLoS ONE 14(8): e0220058. https://doi.org/10.1371/journal.pone.0220058

Editor: Hui Zhao, Guangdong Ocean University, CHINA

Received: February 1, 2019

Accepted: July 7, 2019

Published: August 6, 2019

Data Availability Statement: The data used in this study are freely available from the following websites: 1) Satellite remote sensing Chl-a and SST data were derived from MODIS-Aqua products of NASA (https://oceancolor.gsfc.nasa.gov/l3/); 2) Multivariate ENSO index were derived from monthly average data of NOAA (http://www.esrl.noaa.gov/psd/enso/).

Funding: This study was supported by the National Natural Science Foundation of China-Shandong joint fund (U1806203), the National Science

Abstract

A time series of satellite data on Chlorophyll-*a* concentration (Chl-*a*) that used ocean color was studied to determine mechanisms of phytoplankton variation in recent decade in the Yellow Sea, China during 2003–2015. The variability patterns on seasonal and inter-annual oscillation periods were confirmed using the Empirical Orthogonal Function (EOF), and Morlet wavelet transform analyses, respectively. The first EOF mode for Chl-*a* was dominated by obvious spring and fall blooms in a spatial pattern that was related to the strong mixing of the water masses from the Yellow Sea Cold Warm Mass (YSCWM) and the Yellow Sea Warm Current (YSWC) in winter. The second EOF mode for Chl-*a* showed an opposite spatial pattern between the northern and southern regions. The temporal coefficient showed differences in the timing of blooms. On an inter-annual scale, Chl-*a* indicated variation at periods of 2–4 years during 2003–2015. Chl-*a* showed a significantly negative correlation with the sea surface temperature ($r = -0.21$, $p<0.01$), with time lags of 4 months (Chl-*a* ahead). Chl-*a* was coupled with El Niño Southern Oscillation (ENSO) events, with a positive correlation ($r = 0.46$, $p<0.01$) at a lag of 3–5 months (ENSO ahead). The present study demonstrated that the variation in phytoplankton biomass was controlled primarily by water mass seasonally, and it was influenced by ENSO events on an inter-annual scale.

Introduction

Marine phytoplankton is responsible for almost half of the primary productivity in the world [1]. What controls their abundance is a key issue for understanding the ocean's biogeochemical cycle. Recent research has shown that global phytoplankton biomass has decreased since the past century, probably due to increased sea surface temperatures [2]. Phytoplankton biomass is affected by different factors at the regional scale [3–4]. Chlorophyll-*a* concentration

Foundation of China (41206166), the Fundamental Research Funds for the Central Universities (2019ZRJC005), the Postdoctoral Science Foundation of China (2017M622180), the Fundamental of Guangdong Key Laboratory of Ocean Remote Sensing (South China Sea Institute of Oceanology Chinese Academy of Sciences) (2017B030301005-LORS1803).

Competing interests: The authors have declared that no competing interests exist.

(Chl-*a*) is the crucial biological parameter for simulating marine phytoplankton biomass [5]. Many driving factors (e.g., monsoons, upwelling, coastal currents, vertical mixing, wind speed, etc.) have also been identified that affect Chl-*a* at a regional scale. Sea surface temperature (SST), which reflects the thermal stratification of the ocean, was related closely to variations in phytoplankton biomass on a seasonal scale [6]. El Niño activity is characterized by anomalous warming of the SST in the tropical Pacific, which is linked to a perturbation of atmospheric circulation patterns known as the Southern Oscillation. This ocean-atmosphere coupling is called the El Niño Southern Oscillation (ENSO) [7]. ENSO is the dominant source of inter-annual climate variability in the tropical Pacific Ocean [8]. Fluctuations in phytoplankton biomass have been linked to inter-annual ENSO variability [9–14]. For instance, Hou et al. [15] found phytoplankton biomass positively correlated to the ENSO events in the Western Pacific Ocean. While, Zhao and Tang [16] found the phytoplankton biomass decreased during 1997–98 and 2002–03 EI Niño events.

The Yellow Sea is a relatively shallow sea and has a mean water depth of only 44 m (Fig 1A). Consequently, the Yellow Sea responds relatively quickly to climate changes [17]; in turn, it influences variability in local climate due to the air-sea feedback process. The Yellow Sea Warm Current (YSWC) flows from the southeast to the north in winter (Fig 1B) [18], and the Yellow Sea Cold Water Mass (YSCWM) (122–125˚ E, 33–37˚ N) is entrenched close to the seabed in summer (Fig 1C) [19]. These features represent the two important physical oceanographic phenomena in the Yellow Sea. Additionally, southward coastal currents flow along the coastal sides of the Yellow Sea in winter, which corresponds to the northward YSWC in the central region [20–21]. The seasonal variation in oceanic phytoplankton biomass has been recognized to change with these water circulations in the Yellow Sea, especially in the YSCWM area [22].

In recent years, researchers have reported the spatio-temporal variability in Chl-*a* over decades using satellite data [2–3, 23]. The variability in Chl-*a* was analyzed not only for the global ocean [24], but it was investigated also in the regional areas using satellite datasets [25–28]. These studies illustrated that climate-driven SST generally showed a negative correlation with Chl-*a*, partly because the increasing SST reduced the nutrients supply from the deep layer [29]. However, the detailed analyses were lacking in the Yellow Sea.

Compared with studies of seasonal changes in phytoplankton biomass in the Yellow Sea, there have been many fewer studies of inter-annual variability in phytoplankton biomass. Three notable exceptions for the Yellow Sea were the studies of Shi and Wang [30] on the seasonal and inter-annual Chl-*a* variability during 2002–2009, of Liu and Wang [31] on the Chl-*a* seasonal trend during 1997–2011, and of Yamaguchi et al. [32] that revealed seasonal and spring inter-annual variations in Chl-*a* during 1998–2007. These above studies focused on seasonal and inter-annual scales on a short period. In this study, combined the updated satellite datasets, we examined the variation in Chl-*a* seasonality during 2003–2015 in the Yellow Sea (30–40˚ N, 118–126˚ E), using the empirical orthogonal function (EOF). Also, the inter-annual temporal correlations between Chl-*a* and SST, and Chl-*a* and multivariate ENSO index (Niño 3.4) were explored using wavelet coherency analysis.

Datasets and methodology

Datasets

The monthly MODIS-Aqua datasets for Chl-*a* and SST from 2003–2015 were used in this study. The Chl-*a* and SST datasets were both level 3 fields at 4 km spatial resolution downloaded on the NASA ocean color webpage (http://oceancolor.gsfc.nasa.gov). The standard Chl-*a* product was derived using the OC3Mv5 algorithm, and the daytime SST 11 μm product

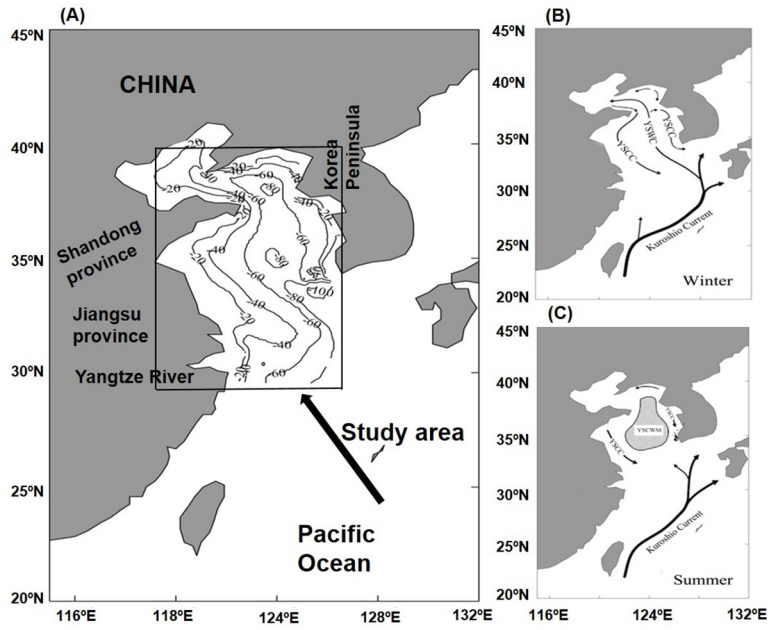

Fig 1. The study area in the Yellow Sea, China. (A) Location of the study area in the Yellow Sea. The isobaths are in meters (same in the below figures). (B) Major water currents during winter in the Yellow Sea. (C) Major water currents during summer in the Yellow Sea. Yellow Sea Coastal Current (YSCC), Yellow Sea Warm Current (YSWC), Yellow Sea Cold Water Mass (YSCWM).

https://doi.org/10.1371/journal.pone.0220058.g001

used the 11 and 12 μm bands. The study area spanned 30–40˚ N in latitude and 118–126˚ E in longitude for the Yellow Sea region. The Niño 3.4 was acquired from NOAA's Earth System Research Laboratory (http://www.esrl.noaa.gov/psd/enso/).

Methodology

Empirical Orthogonal Function (EOF). Because the EOF and wavelet analyses generally require a complete time series of input maps without data voids, the decompositions from Data Interpolating Empirical Orthogonal Functions (DINEOF) were used to obtain complete Chl-*a* and SST datasets [33–34]. DINEOF has been used widely to construct the ocean parameters widely [25, 35–37]. EOF analysis was applied to the monthly Chl-*a* dataset. The dataset was organized in an ($M \times N$) matrix, where M and N represented the spatial and temporal elements, respectively. Prior to EOF analysis, the temporal means in each pixel were removed for Chl-*a* from the original dataset using: $I'(x,t) = I(x,t) - 1/N \sum_{j=1}^{N} I(x,t_j)$, where $I'(x,t)$ are the resulting residuals (anomalies). Alternatively, the spatial means of each pixel were removed using: $I'(x,t) = I(x,t) - 1/M \sum_{j=1}^{M} I(x,t_j)$. For Chl-*a*, the matrix $I(x,t)$ can be written by $I(x,t) = \sum_{n=1}^{N} an(t)Fn(x)$, where $an(t)$ are the temporal evolution functions and $Fn(x)$ are the spatial eigen-functions for each mode.

To assess the significance of the EOF modes, we followed the methods described by North et al. [38]. The error produced in a given EOF (e_j) was calculated as: $e_j = \lambda_j (2/n)^{0.5}$, where λ is the eigenvalue of that EOF and n is the degrees of freedom. When the difference between neighboring eigenvalues satisfied $\lambda_j - \lambda_{j+1} \geq e_j$, then the EOF modes represented by the former eigenvalue were significant statistically. In this study, the first two modes of Chl-*a* passed the significance test. Thus, the first two modes were used to analyze the major variability in this study.

Continuous wavelet transform (CWT). The classical Fourier transform is able to localize the signal only in the frequency domain with no localization in time, but the continuous wavelet transform (CWT) can localize the signal in domains both of time and frequency domains [39]. Therefore, in this study, we used the CWT to determine the oscillation periods of DINEOF Chl-*a* on inter-annual scales. Before the CWT analysis, the seasonal mean calculated from the original dataset was removed from each pixel. The non-stationary time series at different spatial or temporal scales was decomposed into time-frequency space by the CWT, which analyzed localized variations in power and translated the mother wavelet. We used the "Morlet" wavelet as the mother wavelet, which is used commonly in geophysics because it gives a reliable balance between frequency and time localization [40]. Then, the wavelet coherence was used to explore the local correlation between Chl-*a* and SST, and Chl-*a* and Niño 3.4 in time and frequency space.

Results and discussion

Annual mean Chl-*a*

The magnitude of Chl-*a* decreased from coastal waters to offshore regions in the Yellow Sea (Fig 2A). Normally, the highest Chl-*a* values have usually been observed in coastal waters that were adjacent to the mouth of the Yangtze River where the water depth <20 m, and the central Yellow Sea waters had one of the lowest Chl-*a* regions. Chl-*a* variability based on standard deviations (STD) of annual mean temporal values showed that the lowest STDs (~0.02 mg m^{-3}) (Fig 2B) in coastal waters were observed where the highest Chl-*a* values occurred (Fig 2A). The Chl-*a* STD in the area of the YSCWM exhibited high variability, which implied that the dynamic of the YSCWM had influenced the Chl-*a* variation in the central Yellow Sea profoundly.

Seasonal variability in Chl-a

Although the maximum Chl-*a* appeared to be fairly consistent seasonally, the spatial extent of blooms had significant seasonal fluctuations (Fig 3). Monthly mean imagery showed that the largest spatially extent of Chl-*a*, (> 2 mg m^{-3}) was in April (spring), and that the smallest extent was in July (summer) in the Yellow Sea. Chl-*a* in coastal waters (< 50-m isobaths) was relatively high in spring every year. However, some portions of phytoplankton blooms occurred only in subsurface waters, which were impossible to detect using satellite imagery [41]. Overall, the highest Chl-*a* occurred in spring in coastal regions or in regions where the seawater had been diluted greatly by freshwater, such as those close to the Yangtze River mouth, where Chl-*a* was characterized by a long-lasting summer maximum that started in April and ended in September. However, vertical mixing in the water column that was caused by the strong northeast monsoons re-suspended the sediment in this area [42], and, therefore, Chl-*a* was probably overestimated [32, 43].

The EOF was used to analyze the seasonal variability in Chl-*a*. The first and second EOF modes explained 34% and 6% of the total Chl-*a* variability in this study, respectively (Fig 4). The EOF proportions were similar to those observed in previous studies (35% and 47%) on regional and global Chl-*a* [9, 29]. The spatial pattern of the first EOF mode for Chl-*a* was not distributed uniformly throughout the entire study area (Fig 4A). One of the centers of higher Chl-*a* anomalies lay in an area at 35–37˚ N and 122–126˚ E, which was affected mainly by the YSCWM in the central waters of the Yellow Sea [18]. In that location, the strong mixing during winter brought the deeper nutrients upward in the water column, which favored phytoplankton blooms [31]. Another high Chl-*a* center was located in the southeastern region near the YSWC. Thus, we speculate that in the Yellow Sea the water masses from YSCWM and YSWC

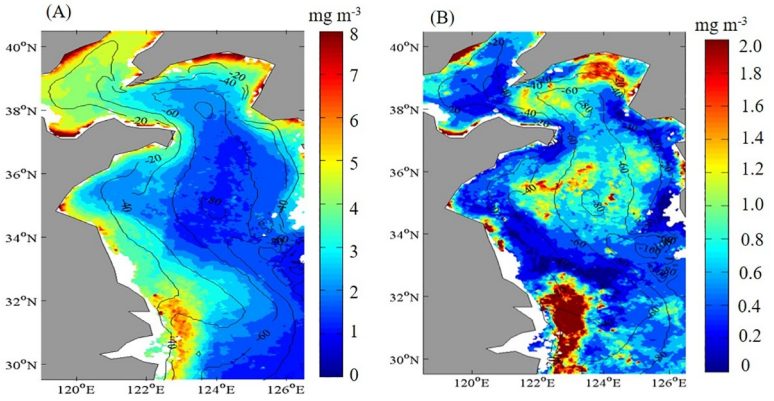

Fig 2. Spatial patterns of temporal means in the Yellow Sea, China. (A) Chlorophyll-*a* concentration (Chl-*a*) and (B) the Chl-*a* standard deviation map during 2003–2015.

https://doi.org/10.1371/journal.pone.0220058.g002

were the main factors that affected the first EOF mode of Chl-*a*. The temporal amplitude showed positive values from winter to spring (November to April) but negative values from summer to fall (June to October) (Fig 4B). The seasonal cycles could be the main reason for this phenomenon, with a high Chl-*a* occurred during winter to spring in offshore regions, and a high Chl-*a* during summer occurred in coastal areas. Also, the subsurface slope water was nutrient rich and, therefore, provided important nutrients from the subsurface to the surface [35]. The spatial pattern of the second EOF mode for Chl-*a* showed a remarkable positive

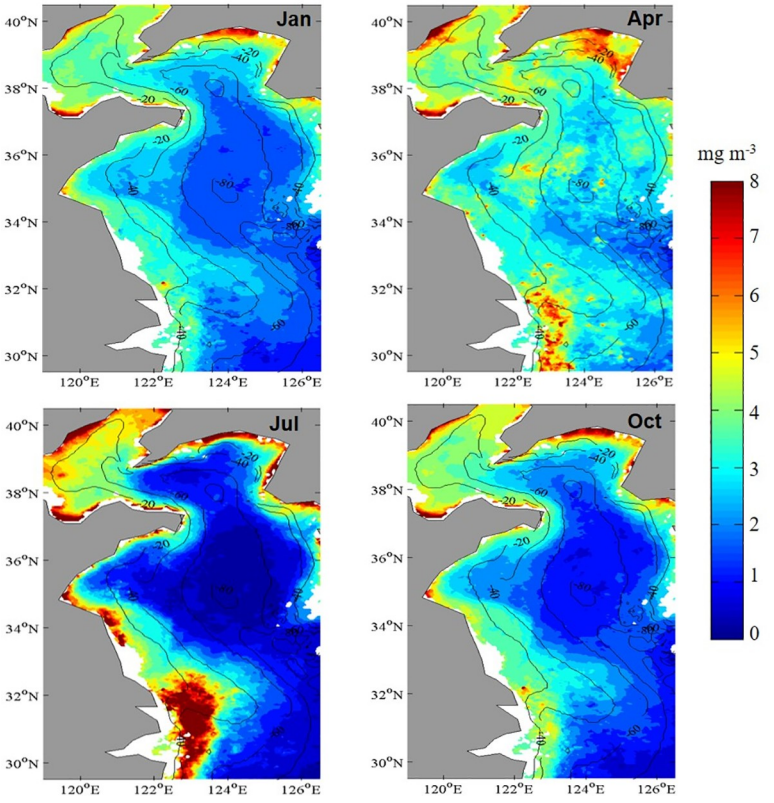

Fig 3. Monthly mean distributions of Chl-*a* during 2003–2015 in the Yellow Sea, China.

https://doi.org/10.1371/journal.pone.0220058.g003

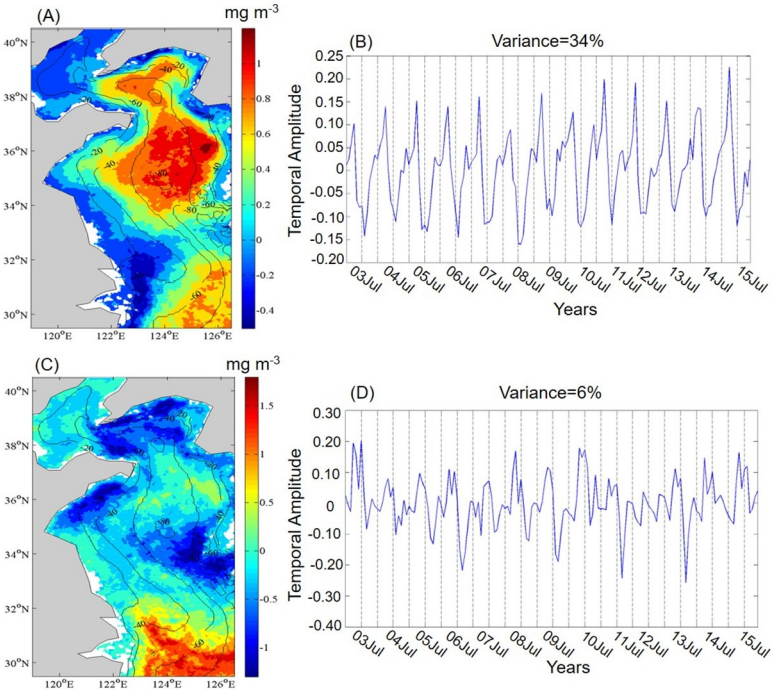

Fig 4. Variability in Chl-*a* during 2003–2015 in the Yellow Sea, China. (A) Spatial pattern and (B) temporal amplitude for the first EOF mode, (C) spatial pattern and (D) temporal amplitude for the second EOF mode.

https://doi.org/10.1371/journal.pone.0220058.g004

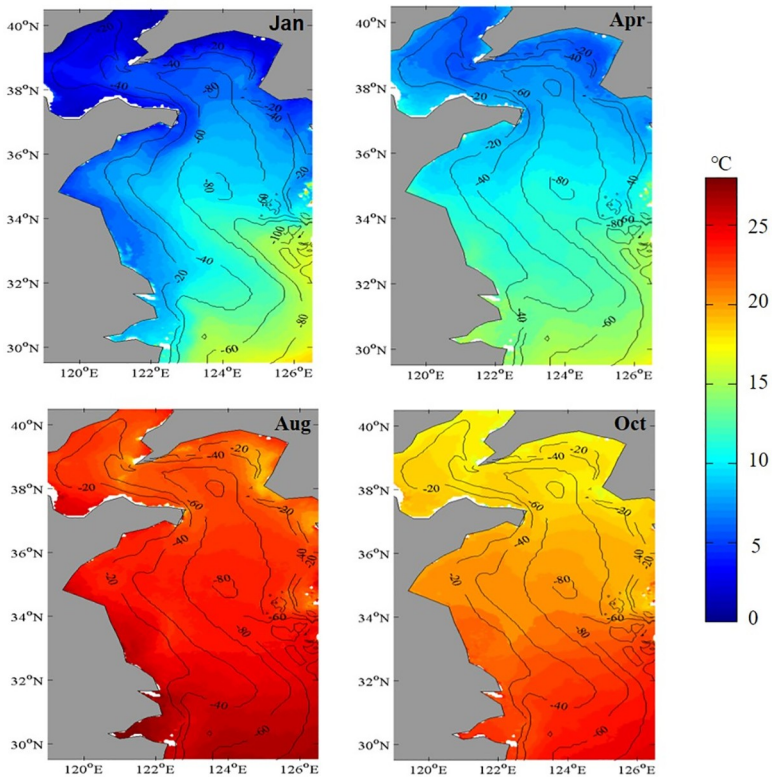

Fig 5. Monthly mean distributions of SST in the Yellow Sea, China during 2003–2015.

https://doi.org/10.1371/journal.pone.0220058.g005

signal in the southeastern Yellow Sea, but a negative signal dominated the northern Yellow Sea (Fig 4C). The second Chl-*a* mode probably represented the differences in the timing of blooms. The distribution of the second Chl-*a* EOF mode differed from that of a previous study by Liu and Wang [31], in which a remarkable positive signal was found in the central area of the Yellow Sea. The temporal amplitude of this mode exhibited a positive signal in spring (March-May) and reached maximum values in June or July. Yamaguchi et al. [32] also detected Chl-*a* maxima in the southeast region during this period.

In the Yellow Sea, the SST presented a sinusoidal seasonal cycle from winter to summer, with a persistent, seasonal warming trend (Fig 5). It showed that the spatial distribution pattern of SST was opposite to that of Chl-*a* in Fig 3 (i.e., the mean Chl-*a* was higher in coastal regions than those in offshore regions, whereas the SST was lower in coastal regions than those in offshore regions). From summer to fall and winter to spring, an indistinct spatial variability was observed both for Chl-*a* and SST. This suggested that the spatial pattern of SST was contrary to that of Chl-*a* to a certain extent. The strong similarity in spatial pattern between the mean Chl-*a* and SST patterns throughout the entire Yellow Sea region was due to lower levels of phytoplankton biomass that corresponded to stronger stratification [23, 44] and the warmer surface waters in the water column [24]. A stratified water column resulted in depleted Chl-*a* in summer, and a less stratified water column resulted in increased Chl-*a* in winter [2, 23, 45]. The decreased/increased stratification was closely related to the enhanced/reduced nutrient availability [46].

Inter-annual variability in Chl-a

The dominant variability scales and oscillation periods of Chl-*a* were highlighted by the Morlet wavelet transform in this study. The global power spectra showed the multi-period for Chl-*a* (right panels of Fig 6A). Chl-*a* exhibited dominant and significant periods of about 1 year and insignificant periods of 3–4 years. The wavelet power spectrum showed that the power of the frequency and amplitude in Chl-*a* anomalies varied with time (left panels of Fig 6A). During 2003–2012, there was a period of variation in Chl-*a* that lasted 1.5–2 years. During 2012–2015, a significant period shift was observed at 3–4 years. Overall, during 2003–2015 Chl-*a* exhibited dominant variations at periods of 1 year and 2–4 years.

The monthly time series of the Chl-*a* anomalies, SST anomalies and Niño 3.4 are displayed in Fig 6B. The Chl-*a* and SST both exhibited increasing trends (Fig 6B), although the Chl-*a*

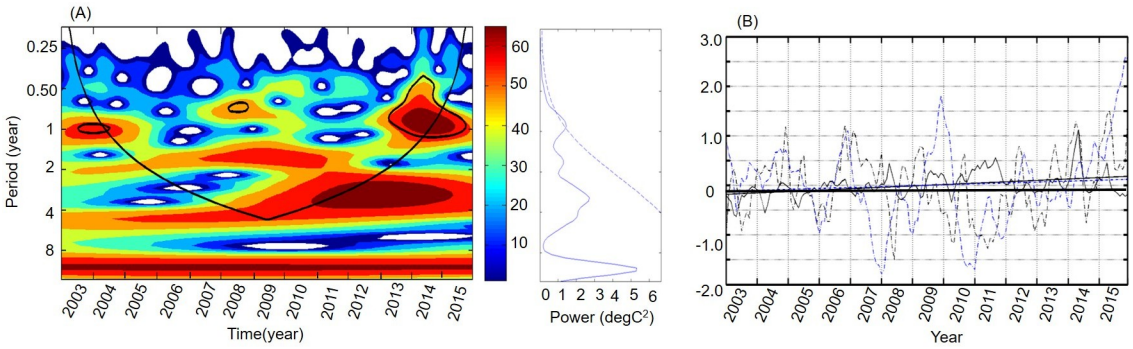

Fig 6. Variation in Chl-*a*, SST, and Niño 3.4 in the Yellow Sea, China. (A) Wavelets of the amplitudes for Chl-*a* after seasonal variation had been removed (the blue dotted line shows the 95% confidence level, and the solid blue line is the global power spectrum in the right panel, respectively). The warm color indicates high power in an arbitrary unit. (B) Time series of mean anomalies for Chl-*a*, SST, and Niño 3.4 (the black lines are Chl-*a* anomalies and least-square linear fits; the black dotted lines are SST anomalies and least-square linear fits; the blue lines are Niño 3.4 and least-square linear fits).

https://doi.org/10.1371/journal.pone.0220058.g006

and SST were still negatively correlated (r = -0.21, p<0.01) in the Yellow Sea, with time lags of 4 months (Chl-*a* ahead). These results agreed well with previous studies, which indicated that SST had a negative relationship with Chl-*a* [14–15, 26]. The correlation of Chl-*a* and Niño 3.4 showed a significant positive correlation (r = 0.46, p<0.01) with a lag of 3–5 months (Niño 3.4 ahead), which suggested that ENSO was probably the dominant factor that drove Chl-*a* variation on an inter-annual scale in the Yellow Sea.

To examine further the synchrony between Chl-*a* with SST and Niño 3.4, wavelet coherence analysis revealed the coherency among them (Fig 7). The wavelet squared coherence values below the confidence level indicated that there were some randomly distributed sections. The vectors indicated the phase difference between Chl-*a* with SST and Niño 3.4 at each time and period, and there was a significant negative coherency between the Chl-*a* and SST during 2008–2015, with a periodicity of 1–2 years (Fig 7A). This coherency period was consistent with the Chl-*a* and Niño 3.4 period at inter-annual scales (Fig 7B).

Concluding remarks

The main purpose of this study was to identify the variability in Chl-*a* on both seasonal and inter-annual time scales and its cross relationship based on long-term, remotely-sensed data. In addition to the EOF, we also applied the wavelet coherency analysis to Chl-*a*, SST, and Niño 3.4 to explore the relationships in a time series for 2003–2015.

On a seasonal time-scale, spatially, Chl-*a* was highest in coastal regions in spring or in regions where the seawater had been diluted greatly by freshwater, and the SST spatial pattern was correlated highly with the distribution of water bathymetry in the Yellow Sea. Temporally, the first EOF mode for Chl-*a* exhibited stronger seasonal variability with a maximum in late winter and early spring and a minimum in summer and early fall, which was affected mainly by the water mass of YSWC and YSCWM. The second EOF mode for Chl-*a* showed differences beginning at the time of blooms. The temporal amplitude exhibited a positive signal in spring (March-May), and it reached maximum values in June or July.

On an inter-annual timescale, Chl-*a* showed dominant variations at periods of 1 year and 2–4 years during 2003–2015. There were increasing trends for Chl-*a* and SST. Furthermore, a significant negative correlation existed between Chl-*a* and SST, but there was a positive correlation between Chl-*a* and Niño 3.4. Thus, on a seasonal scale, phytoplankton variation was controlled mainly by water mass, but on an inter-annual scale, phytoplankton variation was affected by different factors (e.g., water masses, SST, ENSO) in the Yellow Sea.

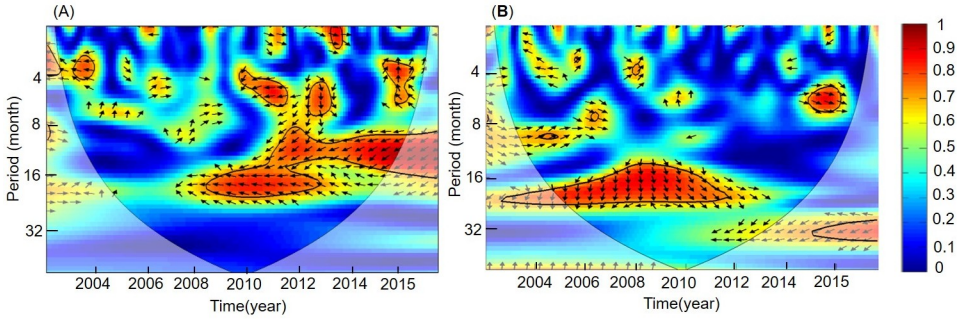

Fig 7. Wavelet coherency analysis of variables in the Yellow Sea, China. (A) Wavelet coherency between Chl-*a* and SST during 2003–2015 in the Yellow Sea. (B) Wavelet coherency between Chl-*a* and Niño 3.4 during 2003–2015. (The thick lines show the 95% confidence levels, and the thin lines separate the cones of influence. The color bar indicates the intensity of the correlation, and the direction of arrows show the correlation type with the right-pointing arrows being positive and left pointing arrows being negative).

https://doi.org/10.1371/journal.pone.0220058.g007

Acknowledgments

We thank NASA's Ocean Color Working Group for providing MODIS-Aqua data, NOAA for ENSO data. The authors appreciate greatly two anonymous reviewers' helpful comments and Dr. J. Owens for language improvement.

Author Contributions

Conceptualization: Chunli Liu.

Data curation: Qiwei Sun.

Formal analysis: Chunli Liu, Qianguo Xing.

Methodology: Chunli Liu, Sufen Wang.

Software: Chunli Liu, Donghe Zhu.

Supervision: Danling Tang.

Visualization: Chunli Liu, Qiwei Sun.

Writing – original draft: Chunli Liu.

Writing – review & editing: Chunli Liu, Danling Tang, Xiang Xing.

References

1. Field CB, Behrenfeld MJ, Randerson JT, Falkowski P. Primary production of the biosphere: integrating terrestrial and oceanic components. Science. 1998; 281: 237–240. https://doi.org/10.1126/science.281.5374.237 PMID: 9657713
2. Boyce DG, Lewis MR, Worm B. Global phytoplankton decline over the past century. Nature. 2010; 466: 591–596. https://doi.org/10.1038/nature09268 PMID: 20671703
3. Gregg WW, Casey NW, McClain CR. Recent trends in global ocean chlorophyll. Geophys. Geophysical Research Letters. 2005; 32: 259–280.
4. Edwards M, Philip Reid, Planque B. Long-term and regional variability of phytoplankton biomass in the Northern Atlantic (1960–1995). ICES Journal of Marine Science. 2001; 58: 39–49.
5. Gregg WW, Conkright ME, Ginoux P, O'Reilly JE, Casey NW. Ocean primary production and climate: global decadal changes. Geophysical Research Letters. 2003; 30: 1809–13.
6. He R, Chen K, Moore T, Li M. Mesoscale variations of sea surface temperature and ocean color patterns at the Mid-Atlantic Bight shelf break. Geophysical Research Letters. 2010; 37: L09607.
7. Racault M-F, Sathyendranath S, Nrewin RJW, Raitsos D, Jackson T, Platt T. Impact of El Niño Variability on Oceanic Phytoplankton. Frontiers in Marine Science.2017; 4: 133. https://doi.org/10.3389/fmars.2017.00133
8. Rousseaux CS, Gregg WW. Climate variability and phytoplankton composition in the Pacific Ocean. Journal of Geophysical Research. 2012; 117: C10006.
9. Messié M, Radenac M-H. Seasonal variability of the surface chlorophyll in the western tropical Pacific from SeaWiFS data. Deep-Sea Research Part I Oceanography Research Papers. 2006; 53 (10): 1581–1600.
10. Park J-Y, Kug J-S, Park J, Yeh S-W, Jang C-J. Variability of chlorophyll associated with El Niño-Southern Oscillation and its possible biological feedback in the equatorial Pacific. Journal of Geophysical Research. 2011; 116: C10.
11. Henson SA, Sarmiento Dunne JP, Bopp L, Lima I, Doney SC, Beaulieu C. Detection of anthropogenic climate change in satellite records of ocean chlorophyll and productivity. Biogeosciences, 2010; 7: 621–640.
12. Tseng C-M, Gong G-C, Wang L-W, Liu K-K, Yang Y. Anomalous biogeochemical conditions in the northern South China Sea during the El-Niño events between 1997 and 2003. Geophysical Research Letter. 2009a; 36: L14611.
13. Shiozaki T, Chen YLL. Different mechanisms controlling interannual phytoplankton variation in the South China Sea and the western North Pacific subtropical gyre: A satellite study. Advances in Space Research. 2013; 52: 668–676.

14. Matsumoto K, Furuya K. Variations in phytoplankton dynamics and primary production associated with ENSO cycle in the western and central equatorial Pacific during 1994–2003. Journal of Geophysical Research. 2011; 116: C12042.
15. Hou XY, Dong Q, Xue CJ, Wu SC. Seasonal and interannual variability of chlorophyll-*a* and associated physical synchronous variability in the western tropical Pacific. Journal of Marine System. 2016; 158: 59–71
16. Zhao H., Tang DL. Effect of 1998 El Niño on the distribution of phytoplankton in the South China Sea. Journal of Geophysical Research. 2007; 112: C02017.
17. Lie HJ, Cho HC, Lee S. Tongue-shaped frontal structure and warm water intrusion in the southern Yellow Sea in winter. Journal of Geophysical Research. 2009; 114: 362–370.
18. Yu F, Zhang ZX, Diao XY, Guo JS. Observational evidence of the Yellow Sea Warm Current. Chinese Journal of Oceanology Limnology. 2010; 28: 677–683.
19. Zhang SW, Wang QY, Lü Y, Cui H, Yuan YL. Observation of the seasonal evolution of the Yellow Sea Cold Water Mass in 1996–1998. Continental Shelf Research. 2008; 28: 442–457.
20. Wei QS, Li XS, Wang BD, Fu MZ, Ge RF, Yu ZG. Seasonally chemical hydrology and ecological responses in frontal zone of the central southern Yellow Sea. Journal of Sea Research. 2016; 112: 1–12.
21. Xu M, Liu QH, Zhang ZN, Liu XS. Response of free-living marine nematodes to the southern Yellow Sea Cold Water Mass. Marine Pollution Bulletin. 2016; 105: 58–64. https://doi.org/10.1016/j.marpolbul.2016.02.067 PMID: 26965091
22. Chu P, Chen YC, Kuninaka A. Seasonal variability of the Yellow Sea/East China sea surface fluxes and thermohaline structure. Advance Atmospheric Science. 2005; 22: 1–20.
23. Behrenfeld MJ O'Malley RT, Siegel DA. Climate-driven trends in contemporary ocean productivity. Nature. 2006; 444: 752–755. https://doi.org/10.1038/nature05317 PMID: 17151666
24. Wilson C, Coles VJ. Global climatological relationships between satellite biological and physical observations and upper ocean properties. Journal of Geophysical Research. 2005; 110: 1–14.
25. Volpe G, Nardelli BB, Cipollini P, Santoleri R, Robinson IS. Seasonal to interannual phytoplankton response to physical processes in the Mediterranean Sea from satellite observations. Remote Sensing of Environment. 2012; 117: 223–235.
26. Gao S, Wang H, Liu GM, Li H. Spatio-temporal variability of chlorophyll-a and its responses to sea surface temperature, winds and height anomaly in the western South China Sea. Acta Oceanological Sinica. 2013; 32: 48–58.
27. Li YZ, He RY. Spatial and temporal variability of SST and ocean color in the Gulf of Maine based on cloud-free SST and chlorophyll reconstructions in 2003–2012. Remote Sensing of Environment. 2014; 144: 98–108.
28. Moradi M, Kabiri K. Spatio-temporal variability of SST and Chlorophyll-*a* from MODIS data in the Persian Gulf. Marine Pollution Bulletin. 2015; 98: 14–25. https://doi.org/10.1016/j.marpolbul.2015.07.018 PMID: 26187398
29. Thomas AC, Strub PT, Weatherbee RA, James C. Satellite views of Pacific chlorophyll variability: comparisons to physical variability, local versus nonlocal influences and links to climate indices. Deep-Sea Research part II-Topical Studies in Oceanography. 2012; 77–80: 99–116.
30. Shi W, Wang M. Satellite views of the Bohai Sea, Yellow Sea, and East China Sea. Progress in Oceanography. 2012; 104: 30–45.
31. Liu DY, Wang YQ. Trends of satellite derived chlorophyll a (1997–2011) in the Bohai and Yellow Seas, China: Effects of bathymetry on seasonal and inter-annual patterns. Progress in Oceanography. 2013; 116: 154–166.
32. Yamaguchi H, Kim HC, Son YB, Kim SW, Okamura K, Kiyomoto Y. Seasonal and summer interannual variations of SeaWiFS chlorophyll *a* in the Yellow Sea and East China Sea. Progress in Oceanography. 2012; 105: 22–29.
33. Beckers JM, Rixen M. EOF calculations and data filling from incomplete oceanographic datasets. Journal of Atmospheric and Oceanic Technology. 2003; 20(12): 1839–1856.
34. Beckers JM, Barth A, Alvera-Azcárate A. DINEOF reconstruction of clouded images including error maps-application to the sea surface temperature around Corsican Island. Ocean Science. 2006; 2: 183–199.
35. Liu M, Liu X, Ma A, Li T, Du Z. Spatio-temporal stability and abnormality of chlorophyll-a in the Northern South China Sea during 2002–2012 from MODIS images using wavelet analysis. Continental Shelf Research. 2014; 75: 15–27.

36. Alvera-Azcárate A, Vanhellemont Q, Ruddick K, Barth A, Beckers JM. Analysis of high frequency geostationary ocean colour data using DINEOF. Estuarine, Coastal and Shelf Science. 2015; 159: 28–36.

37. Huynh HNT, Alvera-Azcárate A, Barth A, Beckers JM. Reconstruction and analysis of long-term satellite-derived sea surface temperature for the South China Sea. Journal of Oceanography. 2016; 72(5): 707–726.

38. North GR, Bell TL, Cahalan RF, Moeng FJ. Sampling errors in the estimation of empirical orthogonal functions. Monday Weather Review. 1982; 110(7): 699–706.

39. Olita A, Ribotti A, Sorgente R, Fazioli L, Perilli A. SLA-chlorophyll-a variability and covariability in the Algero-Provençal Basin (1997–2007) through combined use of EOF and wavelet analysis of satellite data. Ocean Dynamics. 2011; 61: 89–102.

40. Grinsted A, Moore JC, Jevrejeva S. Application of the cross wavelet transform and wavelet coherence to geophysical time series. Nonlinear Process in Geophysics. 2004; 11: 561–566.

41. Townsend DW, Rebuck ND, Thomas MA, Karp-Boss L, Gettings RM. A changing nutrient regime in the Gulf of Maine. Continental Shelf Research. 2010; 30: 820–832.

42. Xie SP, Hafner J, Tanimoto Y, Liu WT, Tokinaga H, Xu H. Bathymetric effect on the winter sea surface temperature and climate of the Yellow and East China Seas. Geophysical Research Letters. 2002; 29: 2228–2231.

43. Siswanto E, Tang J, Yamaguci H, Ahn YH, Ishizaka J, Yoo S, et al. Empirical ocean color algorithms to retrieve chlorophyll-*a*, total suspended matter, and colored dissolved organic matter absorption coefficient in the Yellow Sea and East China Sea. Journal of Oceanography. 2011; 67: 627–650.

44. Doney SC. Oceanography-Plankton in a warmer world. Nature. 2006; 444: 695–696. https://doi.org/10.1038/444695a PMID: 17151650

45. Miles TN, He R. Temporal and spatial variability of CHL and SST on the South Atlantic Bight: Revisiting with cloud-free reconstructions of MODIS satellite imagery. Continental Shelf Research. 2010; 30: 1951–1962.

46. Qiu F, Fang W, Fang G. Seasonal-to-interannual variability of chlorophyll in central western South China Sea extracted from SeaWiFS. Chinese Journal of Oceanology and Limnology. 2011; 29: 18–25.